TIME DEPENDENT DEFORMATION BEHAVIORS AND FATIGUE OF Si_3N_4 CERAMICS AT ELEVATED TEMPERATURES

K. HATANAKA and K. OSHITA
Department of Mechanical Engineering, Yamaguchi University,
2557 Tokiwadai, Ube City, 755 Japan
and
H.SHIOTA
Department of Mechanical Engineering, Gifu University,
1-1 Yanagido, Gifu City, 501-11 Japan

ABSTRACT

The tensile stress-strain response and creep strain of the sintered silicon nitride ceramics were measured in the self-designed projection-accompanied specimen by means of the laser-beam-type extensometer at elevated temperatures. Elastic-plastic and creep finite element analyses were performed for the projection-accompanied specimen. Then the procedure for determining the correct stress-strain response and minimum creep strain rate at elevated temperatures was proposed on the basis of the F.E.M. calculations, using the projection-accompanied specimen. In addition push-pull fatigue test was performed under cyclic stresses with different wave forms at elevated temperatures. It was found from the tests that the fatigue life estimated by the equivalent time is almost independent of the stress wave form and nearly coincide with the static fatigue life.

KEYWORDS

Silicon nitride ceramics, Elevated temperatures, Time dependent stress-strain response, Tensile creep, Push-pull fatigue, Finite element method, Projection-accompanied specimen

INTRODUCTION

A good understanding of high temperature tensile stress-strain response, creep and fatigue of ceramics materials is strongly demanded to promote their application to high temperature machine components. Our knowledge on such basic mechanical properties, however, is extremely limited at present, mainly due to the difficulty in performing experimental work at elevated temperatures over 1000℃.

The authors proposed the method for measuring the strain under tensile loading and the tensile creep strain, using the specimen with four projections which works as the targets for the

scanning laser beam (Hatanaka and Shiota, 1992). The push-pull cyclic fatigue test system has also been developed for testing ceramics materials at elevated temperatures over 1000℃ by the authors (Hatanaka et al, 1994).

The stress/strain analysis is necessitated for the projection-accompanied specimen, since the stress/strain concentration around the root of the projection influences the displacement measured between the two projections under tensile loadings. Meanwhile, cyclic fatigue is expected to be affected by glassy layer softened at grain boundary in Si_3N_4 ceramics at elevated temperatures.

The present paper is concerned with the determination of the time dependent tensile stress-strain response and tensile creep property by using the projection-accompanied specimen and the laser-beam-type extensometer, and the cyclic frequency and stress wave effects on push-pull fatigue of Si_3N_4 ceramics at elevated temperatures.

TEST PROCEDURE

The used silicon nitride ceramics material was fabricated as follows; Y-α sialon and Si_3N_4 particles were mixed at ratio of 40 and 60 weight percents, and then sintered in N_2-gas atmosphere at 1750℃.

Figures 1 (a) and (b) show specimens used for static tensile loadings and push-pull fatigue tests, respectively. The specimen for static tensile loadings has four projections which works as targets for detecting the tensile displacement by means of the laser-beam-type extensometer. The tensile loading and tensile creep tests were performed at elevated temperatures over 1000℃ in air, using the closed loop type hydraulic test system. The displacement rate of the actuator was controlled at $\dot{\delta}$ =0.6, 0.06 and 0.006mm/min in the tensile loading test. The tensile displacement was continuously measured between the two projections on either side of the specimen by means of the laser-beam-type extensometer during tensile loading and tensile creep tests.

The push-pull fatigue test was performed using an another closed loop type hydraulic test system. The stress rate and the stress wave form effects on cyclic fatigue were examined at stress ratio R= − 1.0 under stress controlled condition at elevated temperatures over 1000℃; the triangular stress wave with the stress rate $\dot{\sigma}=10^4$MPa/sec, and the trapezoidal stress waves with hold time on both tension and compression sides and on only tension side were employed in the fatigue test.

TEST RESULTS AND CONSIDERATION

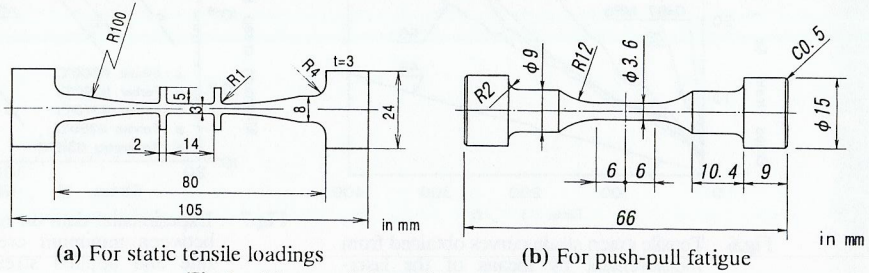

(a) For static tensile loadings **(b)** For push-pull fatigue

Fig.1 Shape and dimensions of test specimen

Tensile Stress-Strain Response

The tensile displacement δ_S was continuously measured between the two projections in the specimen by means of the laser-beam-type extensometer during the tensile loading. The measured relationship between the load P and the displacement δ_S was transformed into the nominal stress-strain response from dividing the load and the displacement by initial cross-sectional area and the initial distance between the two projections of the specimen, and this was shown in Fig.2. According to the figure, the relationship between nominal stress σ and nominal strain ε is expressed by a single linear line at room temperature, independent of the displacement rate. The σ-ε response deviate from the linear to a convex forms at the displacement rate $\dot{\delta}$ =0.006mm/min at 1200℃, while the linear response holds at $\dot{\delta}$ =0.6 and 0.06mm/min at this test temperature. The σ-ε relationship deflects in a convex way at all displacement rates at test temperatures over 1200℃, exhibiting occurrence of inelastic deformation. Furthermore , the yield stress lowers with increase in test temperature and decrease in displacement rate under these test conditions. The elongation before final failure is greatest at $\dot{\delta}$ =0.006mm/min of the three displacement rates at the respective test temperatures of T=1200, 1300 and 1400℃, and becomes larger at the higher test temperature for a given displacement rate.

The tensile strain determined from the displacement measured between the two projections includes the stress/strain concentration effect which should be corrected. Figure 3 shows the tensile stress-strain response obtained from controlling the movement of the actuator of the testing machine at the displacement rate $\dot{\delta}$ =0.06mm/min at the test temperature T=1300℃. The solid line represents the nominal tensile stress-strain curve shown in Fig.2. The relationship between load P and displacement δ_S was calculated for the specimen shown in Fig.1 (a) by elastic-plastic finite element method in which the nominal stress-strain response shown in Fig.3 was employed as the constitutive material's property. The calculated P-δ_S response was shown together with the measured P-δ_S curve in Fig.4. Some difference is found between the two as one expected; stress/strain concentration occurring around the root of the projection is disregarded in the nominal stress-strain response used for the calculation.

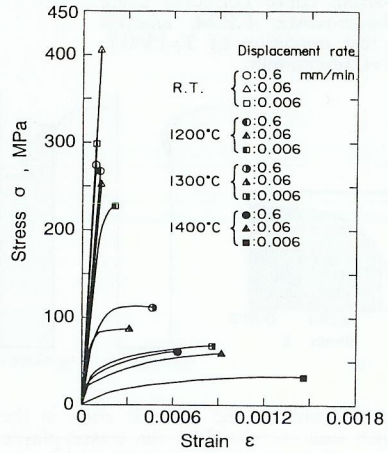

Fig.2 Stress-strain curves at various test temperatures and displacement rates.

The nominal stress-strain response was corrected taking account of the stress/strain concentration around the projection-root in the following way; the nominal stress-strain curve measured in the projection-accompanied specimen was modified into the one which makes the calculated P-δ_s response coincide with the measured P-δ_s response as the constitutive material property in the F.E.M.. The stress-strain curve modified in this way is shown by the dashed line in Fig.3, and this seems to express the correct stress-strain response of the Si_3N_4 ceramics at 1300℃. According to the comparison between the dashed and solid lines shown in Fig.3, the measured nominal strain is about 10 to 15 percent larger than the corrected strain at a given stress level.

The development of elastic-plastic deformation was calculated in the projection-accompanied specimen under tensile loading using the elastic-plastic finite element method, where the corrected stress-strain response was employed as the basic material property. Figures 5 (b) to (e) show the progress of the plastic deformation calculated for a quarter of the specimen subjected to tensile load at $\dot{\delta}$ =0.06mm/min and at T=1300℃. The corrected stress-strain curve is presented again in Fig.5 (a), being demarcated into the seven strain ranges. Then the development of the plastic deformation is expressed by the partition marks shown in Fig.5 (a) in Figs.5 (b) to (e).

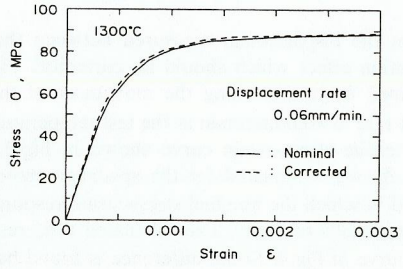

Fig.3 Comparison between the nominal stress-strain curve determined from the measured P-δ_s curve and the stress-strain curve corrected using the elastic-plastic F.E.M. analysis under test condition of T=1300℃ and $\dot{\delta}$ =0.06mm/min.

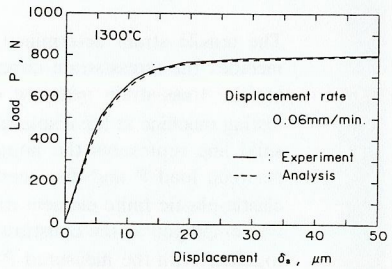

Fig.4 Comparison between the load-displacement curves measured in experiment and calculated through the elastic-plastic F.E.M. analysis using the nominal stress-strain response under test condition of T=1300℃ and $\dot{\delta}$ =0.06mm/min.

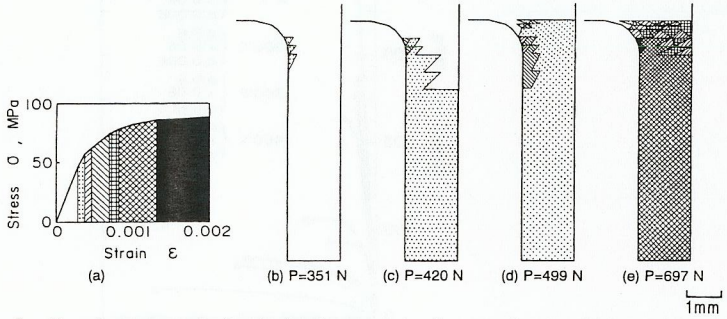

Fig.5 Development of the inelastic zone in the specimen with projections, which was calculated by the elastic-plastic F.E.M. on the basis of the corrected stress-strain response under test condition of T=1300℃ and $\dot{\delta}$ =0.06mm/min. A quarter of the test specimen is presented.

According to Fig.5, the plastic strain first yields in the edge around the root of the projection and then extends to the parallel part of the specimen. Finally this reaches the mid-width section including the specimen axis around the root of the projection. Thus plastic deformation first generated at the root of the projection is restrained from its further development due to the constraint effect of the elastic deformation region retained in the inner-section, and consequently the parallel part of the specimen deforms plastically in advance of the occurrence of gross plastic deformation around the root of the projection. Quite small difference between the corrected and the measured stress-strain responses shown in Fig.3 is due to the restriction of the plastic deformation at the root of the projection from its further development by less strained region retained in the inner section around the root of the projection.

Creep

High temperature tensile creep displacement was measured at several stress levels in the same way as in the measurement of the displacement under high temperature tensile loading. Then the tensile creep strain ε_c was obtained from dividing this by the initial distance between the two projections. The measured creep strains are plotted against test time t in Fig.6, where the upper ends of the curves correspond to the failure points except the one at σ=48MPa which is cut off at t=400hours. The slope of the creep curve was calculated at its steady stage and the minimum creep strain rate $\dot{\varepsilon}_c$ was obtained at the respective stresses. It is known that the minimum creep strain rate is related to stress by the equation $\dot{\varepsilon}_c = K\sigma^n$, where K is a constant and n the power exponent of stress. The minimum creep strain rates obtained from Fig.6 were plotted against stress on double logarithmic scales by open circles in Fig.7. Then the least square's regression analysis was made for these experimental data, and the equation

$$\dot{\varepsilon}_c = 1.37 \times 10^{-15} \sigma^{4.09} \quad (\mathrm{sec}^{-1}) \tag{1}$$

was determined, which is shown by the solid line in Fig.7. The experimental data on the relationship between $\dot{\varepsilon}_c$ and σ (Gürtler, 1991; Ferber and Jenkins, 1992; Tanaka et al, 1991; Kossowsky et al, 1975), which have been obtained at test temperatures around 1300 ℃ before now are

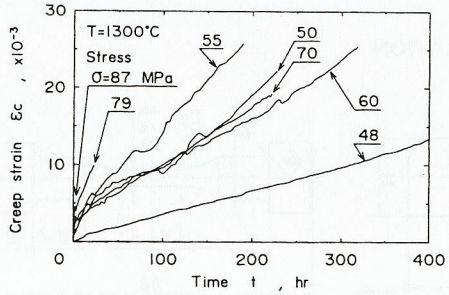

Fig.6 Tensile creep strain curves obtained from measurement by means of the laser-beam-type extensometer, at T=1300℃.

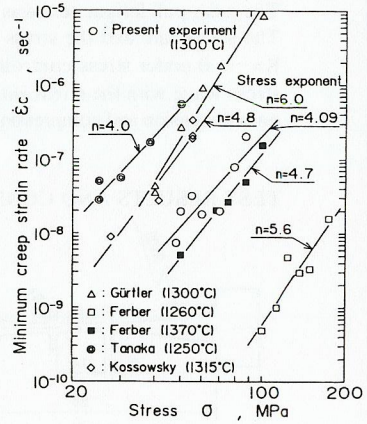

Fig.7 Experimental data on relationship between minimum creep strain rate and applied stress, which were obtained around T=1300℃ before now.

collected in Fig.7, together with the present data. According to the figure, the present $\dot{\varepsilon}_c$ versus σ plots are in reasonable location among the other data, and the power exponent of stress, n=4.09 is also in the range from 4.0 to 6.0 reported by the other researchers.

The steady state creep finite element analysis was performed for the specimen with four projections as follows; first the stress-strain response was calculated by elastic-plastic F.E.M. analysis using the tensile stress-strain curve obtained at 1300℃ which is shown by the dashed line in Fig.3. Then this was followed by the steady state creep F.E.M. analysis in which eq.(1) was employed as the constitutive equation. The minimum creep strain rates calculated at σ=50, 60, 70 and 87MPa in this way are plotted against stress by open triangles in Fig.8. They are in very good agreement with the solid line expressed by eq.(1). This suggests that the measured minimum creep strain rate is hardly influenced by stress/strain concentration induced at the root of the projections. This shows that we can determine the correct relationship between $\dot{\varepsilon}_c$ and σ with practical precision without any corrections, using the tensile specimen shown in Fig.1 (a).

The progress of creep deformation was calculated for a quarter of the tensile specimen subjected to the stress σ=60MPa at T=1300℃ by means of the F.E.M. stated before. Figure 9 shows the change in equivalent creep strain rate $\dot{\varepsilon}_c^{eq}$ in a quarter of the specimen with increase in test time t; (a) to (d) are the creep strain rate distributions at $t=1.0\times10^{-7}$, 0.65, 3.02 and 14.4hours,

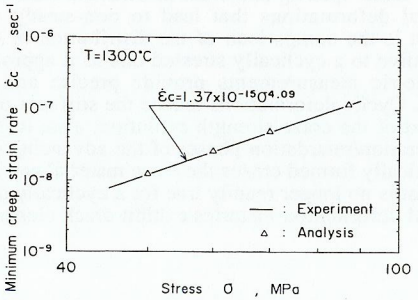

Fig.8 Comparison of the constitutive equation (1) determined from experiment and the relationship between minimum creep strain rate and stress calculated through the F.E.M. using this equation.

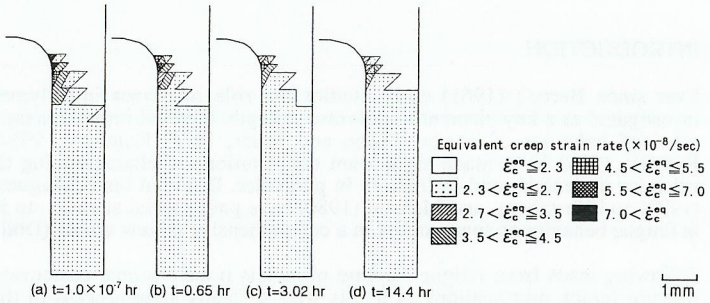

Fig.9 Change in distribution of equivalent creep strain rate in the creep process at σ=60MPa at T=1300℃, which was calculated through F.E.M.. A quarter of the test specimen is presented.

respectively. Just after stress application the high strain rate is locally developed at the root of the projection, as shown in (a); the value of $\dot{\varepsilon}_c^{eq}$ at the root of the projection is about 3.2 times as much as the one at the parallel part of the specimen. The high strain rate attenuates with a lapse of test time due to a stress relaxation occurring around the root of the projection, as shown in (a) to (d). Then the magnitude of $\dot{\varepsilon}_c^{eq}$ at the root of the projection reduces from 3.2 to 1.6 times the one in the parallel part of the specimen with increase in test time from 1.0×10^{-7} to 14.4hours, where the material is in the stage of steady state creep at t=14.4hours. In addition, the domain occupied with high strain rate diminishes as test time elapses. Furthermore, it should be noticed that the region of quite small strain rate is still left in the mid-width section around the root of the projection at t=14.4hours. The very good agreement of the open triangles with the solid line is resulted from such a characteristic progress of the creep deformation in the projection-accompanied specimen.

Cyclic Push-Pull Fatigue

Figure 10 shows the failure life time plotted against stress obtained from static fatigue test at T=1200℃. The least square's regression analysis was conducted for these test data, and then the solid line was determined, which is expressed by the equation,

$$t_s = 6.05\times10^{205}\sigma_s^{-82.6}. \qquad (2)$$

The equation for estimating high temperature cyclic fatigue life time based on the static fatigue test data is derived from the concept that cyclic fatigue failure is caused by extension of defects contained latently in ceramics materials; the static life time equivalent to the cyclic fatigue life t_{eq} was estimated on the basis of S.C.G. concept using eq.(2) (Evans and Wiederhorn, 1974).

The cyclic fatigue tests were performed under the triangular and the trapezoidal stress waves at 1200℃, and the fatigue lives expressed in terms of the number of stress cycles N_f and the equivalent time t_{eq} to failure were plotted against the maximum stress in Figs.11 and 12, respectively. In the figures, the trapezoidal (a) and (b) mean the trapezoidal stress waves with hold time only on the tension side and both on the tension and compression sides. Figure 11 clearly shows that the number of cycles to failure N_f increases with decrease in the hold time. Meanwhile, almost all data points excluding the test data of the specimens failed at the very early time fall around the solid line, showing that cyclic fatigue life is dominated by a time period stressed.

CONCLUSIONS

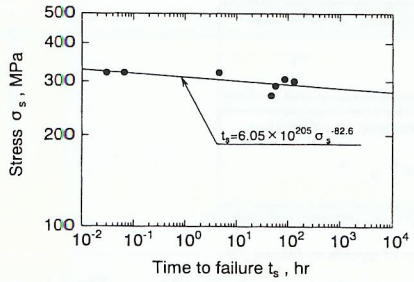

Fig.10 Static fatigue life time obtained from test at 1200℃.

Tensile stress-strain response and tensile creep strain of sintered silicon nitride ceramics were measured in the projection-accompanied specimen by means of the laser-beam-type extensometer at elevated temperatures. Furthermore, push-pull high temperature fatigue test was performed under the controlled several stress waves for this material. Main results obtained are summarized as follows.

(1) Sintered silicon nitride ceramics exhibits non-linear and time dependent stress-strain response at temperatures over 1200℃. The method for correcting the stress-strain curve measured in the projection-accompanied specimen was proposed on the basis of finite element analysis.

(2) It was shown from the creep F.E.M. calculation that the minimum creep strain rate measured in the projection-accompanied specimen might give the correct one with practical precision.

(3) The high temperature fatigue life assessed by the number of stress cycles decreases with increase in the hold time of the trapezoidal stress wave. Meanwhile, the life estimated by the equivalent failure time is little influenced by the stress wave form, and nearly coincides with the static fatigue life.

REFERENCES

Evans, A.G. And Wiederhorn, S.M. (1974). Crack propagation and failure prediction in silicon nitride at elevated temperatures *J. Mater. Sci.*, **9**, 270-278.

Ferber, M.K. and Jenkins, M.G. (1992). Evaluation of the strength and creep-fatigue behavior of hot isostatically pressed silicon nitride. *J. Am. Ceram. Soc.*, **75**, 2453-2462.

Gürtler, M. (1991). Institut für material- und festkörperforschung. *Kernforschungszentrum Kahlsruhe*, KFK-4874.

Hatanaka, K. and Shiota, H. (1992). Tensile stress-strain response of sintered silicon nitride ceramic at elevated temperatures. *Trans. Jpn. Soc. Mech. Eng.*, **58**, 653-660.

Hatanaka, K., Nishimura, H. and Katsuyama, M. (1994). Push-pull cyclic fatigue test of sintered silicon nitride ceramics at elevated temperatures. *Trans. Jpn. Soc. Mech. Eng.*, **60**, 1129-1136.

Kossowsky, R., Miller, D.G. and Diaz, E.S. (1975). Tensile and creep strengths of hot-pressed Si_3N_4. *J. Meter. Sci.*, **10**, 983-997.

Tanaka, T., Okabe, N., Yamamoto, S., Nakayama, H., Segawa, A. and Fujii, T. (1990). Strength and strain behavior in high temperature creep of fine ceramics. *J. Soc. Mat. Sci. Jpn.*, **39**, 1692-1698.

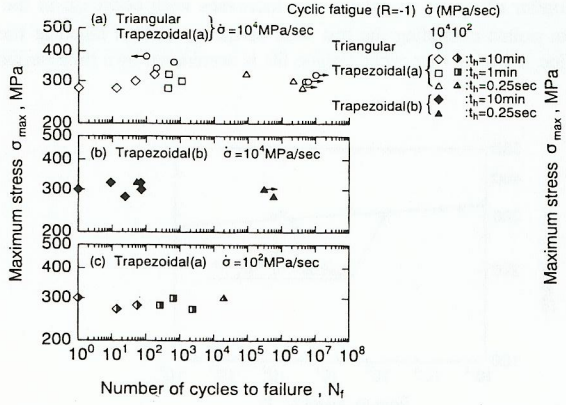

Fig.11 Effect of hold time on cycle-life in cyclic fatigue at 1200℃.

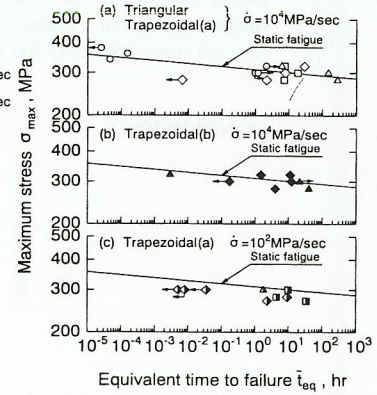

Fig.12 Equivalent time-life vs. maximum stress plots of test data presented in Fig.11.